Nuclear Instruments and Methods in Physics Research B 343 (2015) 116–122

Contents lists available at ScienceDirect

Nuclear Instruments and Methods in Physics Research B

journal homepage: www.elsevier.com/locate/nimb

Combining SAXS and DLS for simultaneous measurements and time-resolved monitoring of nanoparticle synthesis

A. Schwamberger [a,b,*], B. De Roo [d], D. Jacob [c], L. Dillemans [d], L. Bruegemann [b], J.W. Seo [e], J.P. Locquet [d]

[a] TU Dortmund, Experimentelle Physik 1, Otto-Hahn-Str. 4, 44221 Dortmund, Germany
[b] Bruker AXS GmbH, Östliche Rheinbrückenstr. 49, 76187 Karlsruhe, Germany
[c] Cordouan Technologies, Cité de la Photonique, 11 Avenue Canteranne, 33600 Pessac, France
[d] KU Leuven, Department of Physics and Astronomy, Celestijnenlaan 200D, 3001 Heverlee, Belgium
[e] KU Leuven, Department of Metallurgy and Materials Engineering, Kasteelpark Arenberg 44, 3001 Leuven, Belgium

ARTICLE INFO

Article history:
Received 24 September 2014
Received in revised form 10 November 2014
Accepted 14 November 2014

Keywords:
SAXS
In situ DLS
Microflow reactor
Nanoparticles

ABSTRACT

Time-resolved characterization of nano-particle (NP) synthesis is a promising mean to produce NPs under controlled conditions. Here, an innovative experimental demonstration of a NP characterization tool which combines a laboratory Small Angle X-ray Scattering (SAXS) instrument, a new Dynamic Light Scattering (DLS) device and a microflow reactor is shown. The complementary SAXS and DLS techniques were designed and optimized to meet the ambitious requirements of time-resolved monitoring of NP suspensions while ongoing synthesis. For this purpose, SAXS instrument performance was enhanced by the implementation and optimization of a unique X-ray metal jet source. In parallel, an innovative DLS fiber remote probe head was developed specifically for *in situ* measurements. DLS measurements were performed directly inside a 2.0 mm diameter glass capillary located inside the SAXS vacuum sample chamber. The combined SAXS and DLS devices were tested separately on commercially available gold NP suspensions of known size. Furthermore, simultaneous SAXS and DLS measurements were performed during the synthesis of silica NPs.

1. Introduction

The use of nano-particles (NPs) is increasing in science, industry and medicine [1–5]. In most applications, a very good knowledge of the properties of NPs is desired. The targeted physical properties depend strongly on the morphology (size, shape) and the degree of polydispersity. Therefore, the key to obtain NPs with precisely taylored properties is the capability to control and tune their morphology and the size and shape distribution during their synthesis. A way to achieve this is to monitor the synthesis process in a time-resolved manner and apply feedback on the synthesis process. By this means, one can tune the synthesis parameters until the NPs exhibit the desired morphology. For this purpose, a broad range of information on the NPs must be available at a time.

Among the various known characterization techniques used in colloidal science, Small Angle X-ray Scattering (SAXS) and Dynamic Light Scattering (DLS) are certainly the most prevalent, because they are non-invasive and non-destructive. Furthermore, using combined SAXS and DLS yields complementary information, i.e. static and dynamic properties of colloidal NPs in suspension can be investigated. On the one hand, SAXS is a static light scattering technique sensitive to the electron density contrast. In SAXS one measures the time-averaged intensity of the scattered X-rays as a function of the scattering angle. The measured intensity curve bears information on the radius of gyration, mean size, size distribution, shape, number density and scattering volume of the scatterers [6]. Additionally, the fractal structure can be probed by SAXS. This is especially important when investigating the nucleation and growth kinetics of NPs [7]. SAXS is typically utilized to NPs in a size range from 1 nm to 100 nm. On the other hand, DLS is based on the temporal analysis of the intensity fluctuations of the scattered caused by the Brownian motion of the suspended NPs. DLS is sensitive to the refractive index contrast between the NPs and the solvent. It gives information on the dynamic properties of the NPs, i.e. diffusion coefficient and average hydrodynamic radius. DLS allows to determine the average particle size and size distribution in a broad range from a few nanometers up to several microns. However, shape information are not easy to obtain. Thus,

* Corresponding author at: Bruker AXS GmbH, Östliche Rheinbrückenstr. 49, 76187 Karlsruhe, Germany.
E-mail address: alexander.schwamberger@bruker-axs.de (A. Schwamberger).

http://dx.doi.org/10.1016/j.nimb.2014.11.049
0168-583X/

only a combination of both techniques yields an exhaustive image of the NPs by overcoming drawbacks and incapabilities of the individual techniques.

Time-resolved NP monitoring is a challenging task which requires a high level of sophistication and refinement of existing laboratory characterization techniques. Especially the time resolution or the sampling rate of the monitoring process is a crucial parameter which is mainly given by the exposure time. In the view of a feedback-looped NP production a short exposure time ensures fast response after changing the synthesis conditions. Shortening the exposure time in SAXS measurements while preserving a good signal to noise ratio implies to have a high X-ray flux at sample location. In this work, this was achieved by implementing a novel liquid metal anode X-ray source combined with a novel X-ray collimation system with specific pinholes having significantly reduced parasitic edge scattering. The main challenge for the DLS device was to be able to bring the DLS measurement to the sample position, directly inside the SAXS sample chamber. To account for mechanical and integration constraints, an innovative DLS probe was designed. For the synthesis of the silica NPs a microflow reactor was used. The silica NPs were examined directly after the synthesis in a flow-through capillary. SAXS and DLS measurements were performed at the same time and same capillary location.

The complementary use of both techniques has been already reported in the literature [8–10]. However, to the best of our knowledge the feasibility of a simultaneous use of laboratory SAXS and optical fiber based DLS for time-resolved monitoring of NP synthesis is shown here for the first time.

2. Instruments

2.1. SAXS

For the SAXS measurements a Nanostar (Bruker AXS) was used, which features the novel MetalJet X-ray source (Excillum). This X-ray source functions with liquid metal (an alloy of gallium and indium) as target material [11]. The metal is circulating in a loop and a special nozzle produces a jet of 180 μm in diameter which is irradiated with electrons to generate X-rays. By using a liquid and renewable target material one can increase considerably the electron power density compared to solid target X-ray sources. The MetalJet X-ray source is running with 200 W at 70 kV acceleration voltage producing an electron emission current of around 2.8 mA. The electrons are focused down to a focal beam size of 80 × 20 μm^2 (H × V, FWHM) at the jet position. Consequently, the resulting electron power density on the jet is around 125 $\frac{kW}{mm^2}$. State-of-the-art microfocus rotating anode sources have an electron power density of approximately 25 $\frac{kW}{mm^2}$ at 2500 W and 1000 × 100 μm^2 (H × V, FWHM), which is a factor 5 less compared to the MetalJet source. The projected spot size seen by the optic at an angle of 90° with respect to the electron beam and the jet is approximately 20 × 20 μm^2. A more detailed description of the MetalJet X-ray source can be found in [12,13]. A focusing Montel multilayer optics designed to take advantage of the small spot size is used to monochromize the radiation yielding Ga-K_α X-rays of a wavelength of 1.34 Å. A higher electron power density and the small apparent spot size result in a higher brilliance and consequently in higher flux at the sample position. A flux increase of a factor 4 compared to Brukers rotating anode system can be measured. To further increase the X-ray flux on the sample a new X-ray beam collimation pinhole setup was tested. In this setup SCATEX pinholes (Incoatec) were used which exhibit drastically reduced parasitic edge scattering [14]. A schematic drawing of the collimation setup is shown in Fig. 1. For the collimation only two pinholes are used. This is in contrast to a standard SAXS pinhole setup comprising 3 pinholes [15]. Owing to the nearly total absence of the edge scattering the third pinhole becomes obsolete when using SCATEX. Furthermore, the diameter of the beam-defining pinhole was increased from 400 μm to 550 μm and the distance between the first and second pinhole was decreased from 920 mm to 535 mm. This results in a flux increase by approximately a factor of 2.5 compared to the standard pinhole setup. All in all, by using a MetalJet source and SCATEX pinholes the flux at the sample position can be increased by a factor of 10 compared to a rotating anode system with the standard pinhole setup.

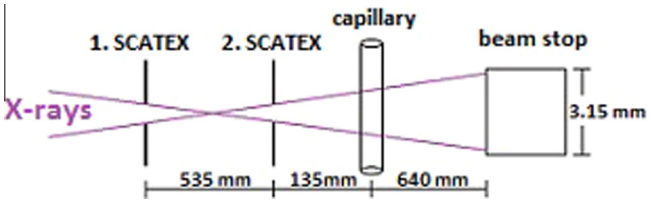

Fig. 1. X-ray beam collimation with two SCATEX pinholes.

2.2. DLS

Standard DLS particle size analyzers require batch sampling, i.e. the sample needs to be injected into a dedicated cuvette placed inside the instrument before measurement. This configuration is appropriate for many laboratory applications, but it cannot be coupled to a SAXS system for simultaneous measurements within the same sample volume. Also sampling in a cuvette can be time consuming, with some risk of sample instability and heterogeneity from batch to batch and related reproducibility issues. These constraints are not compatible with time-resolved process monitoring requirements. This observation implies a change of paradigm: if you cannot bring the sample to the measurement, you have to bring the measurement to the sample; this underlies the original concept of the new DLS probe developed specifically to be integrated into the SAXS sample chamber. Thus, at the heart of the new DLS system is an Optical Fiber Remote Head (OFRH). A schematic drawing is shown in Fig. 2. The OFRH integrates into the same case housing both the sample illumination optical system and the scattered light collector with its optical axis set at an angle of 165° with respect to the incident laser beam propagation axis. The working distance of the probe (i.e. the distance between the probe head and the sample capillary) is set to 70 mm. The illumination and the collector systems are made of two optical collimators, one used as condenser and the other as a focuser. These collimators have been designed and optimized to maximize sensitivity (i.e. the scattering volume) and the signal to noise ratio (i.e.

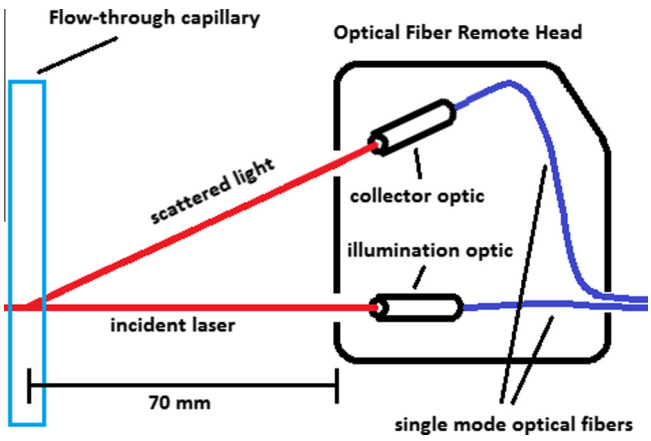

Fig. 2. Schematic drawing of the OFRH. It incorporates the optics for the main laser and the scattered light. The optics are coupled to optical fibers.

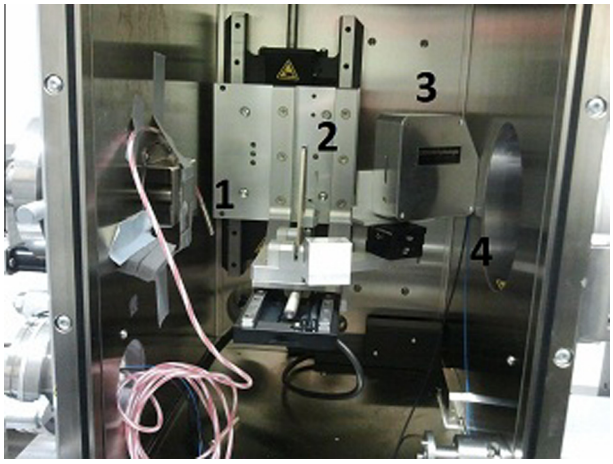

Fig. 3. Optical Fiber Remote Head (top) integrated into the SAXS sample chamber (bottom) with a temperature sensor (1), capillary holder (2) the DLS head (3) and the optical fibers (4).

spatial coherence). The laser beam diameter in the measurement area is about 200 μm. The OFRH is linked to a central unit with an optical fiber patch cord which integrates two single mode fibers: one polarization maintaining fiber used for the laser beam and one standard single mode fiber used to collect the scattered light from the sample to be characterized. The polarization of the laser beam is aligned in a direction perpendicular to the plane of incidence defined by the laser and the collecting beam.

In the current arrangement, for ease of alignment and space constraints reasons, the plane of incidence of the OFRH is parallel to the glass capillary axis (see Fig. 2). Nevertheless, to minimize the contribution of the Doppler shift on the DLS signal induced by the flow, it would be preferable to have the plane of incidence perpendicular to the longitudinal axis of the capillary. This would prevent from stopping the flow during the DLS measurements. Such modification is currently under study.

The central unit includes: a high sensitivity single photon Avalanche PhotoDiode (APD), a high resolution (1000 channels) home-made data processing linear correlator, an external temperature sensor (PT100) and a 60 mW fiber pigtailed laser diode emitting at 658 nm. A fiber pigtailed alignment laser is also coupled to the collecting fiber through a 1×2 optical switch in order to visualize the measurement area during the alignment procedure. Finally, the OFRH is mounted on a XY translation stage in order to optimize the alignment of the DLS probe laser beam within the glass capillary and overlap with the SAXS X-ray beam. Fig. 3 shows the OFRH integrated into the Nanostar sample chamber.

3. Experimental methods

3.1. Chemicals

In this work two experiments are shown. For the first experiment a sample set of three gold NP suspensions with particles of 10 nm, 15 nm and 20 nm in diameter (Cytodiagnostics, standard gold nanoparticles) were used to validate the SAXS and DLS instruments.

In the second experiment, simultaneous SAXS and DLS measurements while ongoing synthesis of silica NPs are performed. Tetraorthosilicate (TEOS, 99.999% Sigma–Aldrich), Ethanol (>99.8%, Fluka) and NH_4OH (28–30%, Acros) were used to synthesize silica NPs. The synthesis is performed via an adaptation of the Stöber method to a microfluidic reaction. The Stöber process can be writen as [16,17]:

$$\mathrm{TEOS} + \mathrm{H_2O} \xrightarrow{\text{hydrolysis}} \mathrm{Si(OH)_4} + \text{ethanol}$$

$$\mathrm{Si(OH)_4} + \mathrm{H_2O} \xrightarrow{\text{condensation}} \mathrm{SiO_2}$$

In the experiment a 75 mM TEOS solution (in ethanol) and a 727 mM aqueous ammonia solution were used.

3.2. Production and characterization of NPs

For the synthesis of NPs a microflow system (Asia 110 Flow Chemistry System from Syrris) was used. This system consists of two syringe pumps, a microflow reactor and a temperature controller for the reactor. The volume of the reactor used in this work is 1000 μl. The flow rates of the two pumps can be varied separately in a range of 10 μl/min – 2.5 ml/min. In Fig. 4 a schematic drawing of the production and characterization line of a NP suspension is depicted. Two syringe pumps inject the two precursors (TEOS in ethanol and ammonia water solution) inside the microflow reactor where the mixing and consequently the synthesis starts. The flow rates F_1 and F_2 of the first pump and the second pump can be varied separately. In this experiment, the flow rate values range from 15 μl/min to 300 μl/min. One important parameter is the flow rate ratio $\frac{F_1}{F_2}$ which affects the mutual concentration, e.g. the amount of TEOS with respect to water and ammonia. Other important parameters are the reactor temperature and the residence time inside the reactor which depends on the total flow rate and the reactor volume and can be given as $\frac{1000\ \mu l}{F_1+F_2}$. In this work, the residence time is varied in the range from 2 min to 22 min, whereas the temperature of the reactor was set to 60°C and kept constant during the experiments. The NPs pass through a home-made glass capillary and get exposed to the X-ray and the laser beam as shown in Fig. 5. Before reaching the capillary the NPs pass through a tube which connects the reactor with the capillary. The volume of the tube is approximately 450 μl, resulting in a delay time between reactor and capillary of one-third of the residence time. This delay cannot be removed completely because the reactor cannot be placed inside the SAXS sample chamber. However, the delay time was minimized by shortening the tube to a certain minimal length.

3.3. SAXS, DLS and TEM measurements

In a first series of experiments, standard gold NPs were measured. The three gold NP suspensions were filled into standard

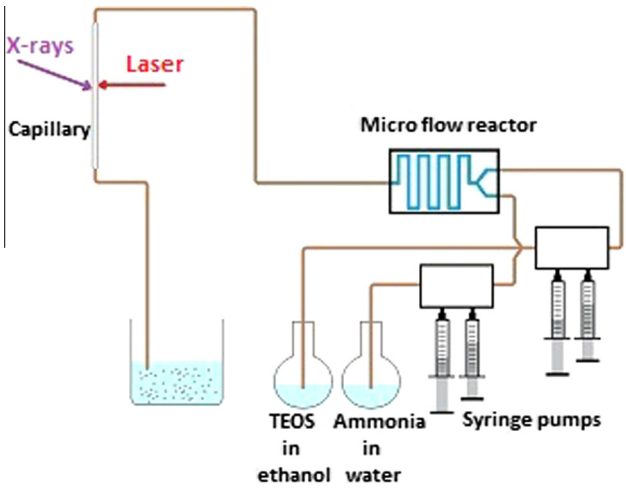

Fig. 4. Schematic drawing of the production and characterization line of a NP suspension.

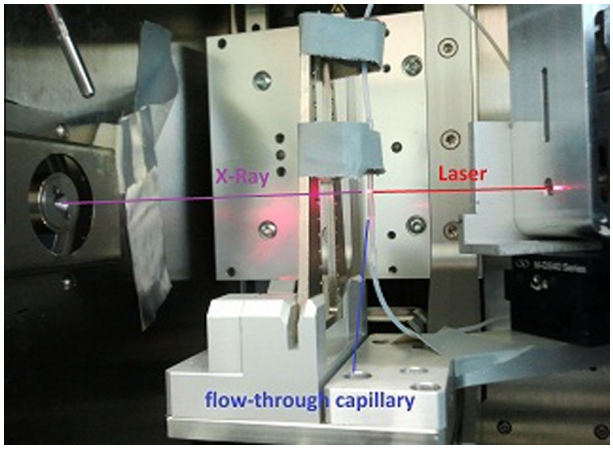

Fig. 5. Flow-through capillary holder inside the SAXS sample chamber. The X-ray and laser beam hit the flow-through capillary at the same position.

capillaries, respectively. The capillaries were then sealed with wax, placed on the capillary holder and measured with SAXS and DLS one after another. In a second series of experiments, the synthesis of silica NPs was performed and the synthesis parameters were changed. Time-resolved monitoring was performed while ongoing synthesis and flow with the SAXS instrument. Every 20 s a 2D-image was taken which was then converted into a 1D curve by azimuthal integration to yield the scattered intensity as a function of the scattering angle. The 1D data points are stored in a file on the computer. Brukers "SAXS-NT" software is the basis for the monitoring with SAXS. The software can be scripted to perform the data collection, integration and the raw data storage automatically and iteratively. For further processing of the raw data a program in Python was written. Every 20 s, when a new raw data file was stored, the program performed a background correction and fitted a function to the measured curve to extract the mean radius R_m and the standard deviation σ of the size distribution. The fit function is calculated according to

$$I(q,R) \propto \int_0^\infty |F(q,R)|^2 D(R,R_m,\sigma) V(R)^2 \mathrm{d}R, \tag{1}$$

where $q = \frac{4\pi}{\lambda} \sin\frac{2\Theta}{2}$ is the modulus of the scattering vector as a function of the wavelength λ and the scattering angle 2Θ defined as the angle between the wavevector of the incident and the wavevector of the scattered beam.

$$F(q,R) = 3\frac{\sin(qR) - qR\cos(qR)}{(qR)^3} \tag{2}$$

is the form factor of a sphere [18]. $V(R)$ is the volume of a sphere with radius R. $D(R,R_m,\sigma)$ is a size distribution function. In this work a Gaussian and a Schulz-Zimm distribution function are used. The Schulz-Zimm distribution is given as [19]

$$D(R) = AR^\alpha e^{-\gamma R} \quad \text{with} \quad A = \gamma^{1+\alpha}/\Gamma(1+\alpha) \tag{3}$$
$$\text{and} \quad \Gamma(x) = \int_0^\infty t^{x-1} e^{-t} \mathrm{d}t.$$

The mean radius R_m and the standard deviation of the size distribution σ are given as

$$R_m = \frac{1+\alpha}{\gamma} \quad \text{and} \quad \sigma = \frac{1+\alpha}{\gamma^2}. \tag{4}$$

For the time-resolved monitoring the Schulz-Zimm distribution turns out to be more appropriate because the integration in Eq. (1) can be performed explicitly [19]. This makes the data extraction time negligibly short.

Moreover, a graphical user interface (GUI) was implemented that shows the evolution of the size properties in a R_m-vs-time and a σ-vs-time diagram, respectively. The diagrams are updated approximately every 20 s. By this means one is able to track the NP size after the synthesis when the NPs reach the capillary. In this manner, observing changes in size upon modifying synthesis parameters becomes convenient.

DLS measurements were achieved with Cordouans NanoQ proprietary software. The hydrodynamic radius is calculated via the Padé-Laplace method. The DLS technique is based on recording the scattered intensity $I(t)$. The intensity fluctuates randomly due to the Brownian motion of the NPs in the suspension. The hydrodynamic radius of NPs is deduced from the intensity fluctuation autocorrelation [20]

$$g^2(q,\tau) = \frac{< I(t)I(t+\tau) >}{< I(t)^2 >}, \tag{5}$$

which can be also written as

$$g^2(q,\tau) = 1 + \beta |g^1(q,\tau)|^2. \tag{6}$$

$g^1(q,\tau)$ is the electromagnetic field correlation function, $q = \frac{4\pi n}{\lambda} \sin\frac{\theta}{2}$ is the modulus of the scattering vector and is a function of the scattering angle θ, which is also defined as the angle between the wavevector of the incident and the wavevector of the scattered beam. n is the refractive index, τ is the delay time and β is the correlation function amplitude at zero delay. One can show that

$$g^1(q,\tau) = \exp(-\Gamma\tau) \tag{7}$$

and the decay rate Γ is connected to the Einstein-Stokes diffusion coefficient D_f via

$$\Gamma = q^2 D_f \tag{8}$$

with

$$D_f = \frac{k_B T}{6\pi\eta R_H}. \tag{9}$$

η is the viscosity of the solvent, k_B the Boltzmann constant, T the temperature and R_H is the hydrodynamic radius. Thus, by fitting exponential decay functions to the autocorrelation function one can extract the hydrodynamic radius which corresponds to the core radius plus the thickness of a solvation shell surrounding the particle. Therefore, the hydrodynamic radius can be considered as an equivalent radius of a bigger sphere with the same diffusion coefficient as the particle.

SAXS and DLS measurements were performed for different synthesis parameters. Upon changing a parameter, the impact on the size was followed by SAXS in the R_m-vs-time and σ-vs-time diagrams by an increase or decrease of the size indicating that the particles synthesized under the current parameters reached the capillary. At this moment, the flow was stopped and the DLS measurement started. The exposure time was a few minutes. While ongoing DLS measurement the SAXS software was gathering SAXS curves and updating the diagrams in the GUI. After the DLS measurement the flow was started again and new synthesis parameters were set. After the NP suspension passed through the capillary it was collected in extra flasks for each synthesis parameter set, respectively.

DLS *ex situ* measurements were performed for a cross check with a standard VASCO Particle Size Analyzer from Cordouan. Before the *ex situ* measurements were performed the suspensions were diluted with water. The cross check serves to investigate whether both DLS devices yield similar results under different conditions, namely undiluted inside the flow-through capillary and diluted.

Additionally, TEM measurements were performed with a transmission electron microscopy (CM 200FEG Philips) operating at 200 kV and used to cross check the SAXS data. The TEM grids were

prepared by placing 8–10 μl of particle solution on a carbon-coated copper grid and dried under ambient conditions. No purification was performed before application to the grids. At least 100 particles were analyzed for determination of the mean radius and standard deviation. The mean radius is determined according $R_m = \frac{1}{N}\sum_{i=1}^{N} R_i$ and the standard deviation is $\sigma = \sqrt{\frac{1}{N}\sum_{i=1}^{N}(R_i - R_m)^2}$. N is the number of particles taken into account for the analysis.

4. Experimental results

4.1. Simultaneous SAXS and DLS measurements

To test and validate the SAXS and DLS instruments, measurements were performed on standard gold NPs of known size. The results of the simultaneous SAXS and DLS measurements at the same time and same sample position are depicted in Fig. 6 and Table 1. The SAXS curves were fitted according to Eq. (1) assuming a Schulz-Zimm and a Gaussian size distribution, respectively. For the sake of clarity the curves are shifted in intensity. Furthermore, one can notice that the DLS correlation functions have different baselines. We attribute this to parasitic scattering arising from contamination or dust particles on the capillary walls, but which have no major impact on the hydrodynamic radius values extracted from the curves. The DLS correlation functions are plotted on a linear time scale because a linear correlator was used. To assess the accuracy of the simultaneous SAXS and DLS measurements, additional TEM measurements were performed separately. The TEM images are illustrated in Fig. 7. Table 1 presents a comparative overview of all results. The results obtained with the Gaussian and the Schulz-Zimm size distribution are very similar. Furthermore, the SAXS results are in good agreement with the TEM results, whereas the size values obtained with DLS are larger by approximately 3–4 nm. This is due to the aforementioned feature of the DLS technique of being sensitive to the hydrodynamic size of the particles. SAXS and DLS measurements can thus give valuable indications on the solvation layer of the synthesized NPs. However, detailed analysis of the solvation shell is not a subject of this work.

Table 1
Summary of SAXS and DLS results with additional TEM results. All size values are given in units of nm. The measurements were performed on Au NPs with three different radii R of 5 nm, 7.5 nm and 10 nm.

R	SAXS (Gauss)		SAXS (Schulz-Zimm)		DLS	TEM	
	R_m	σ	R_m	σ	R_h	R_m	σ
5	5.2	1.0	5.1	1.0	8.5	5.6	0.8
7.5	7.1	0.7	7.0	0.8	11.2	7.6	0.7
10	9.4	1.2	9.9	1.2	12.1	10.3	1.1

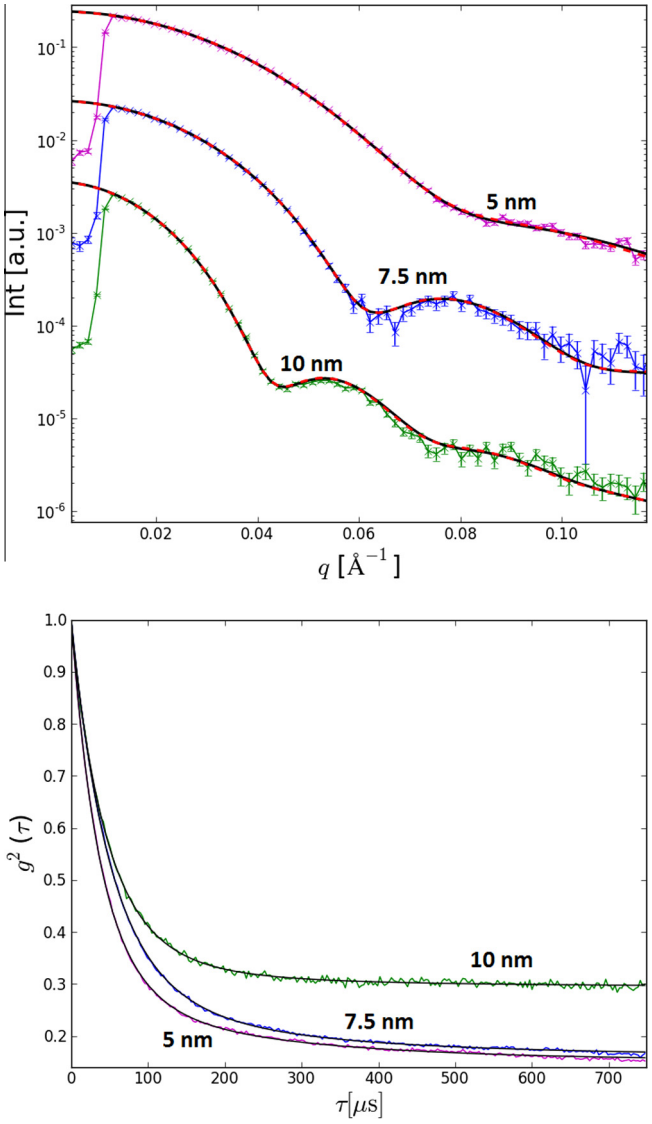

Fig. 6. SAXS measurements (top) and DLS measurements (bottom) on standard gold NPs with radii of 5 nm, 7.5 nm and 10 nm. The SAXS curves were fitted assuming a Schulz-Zimm (solid line) and a Gaussian (red dashed line) size distribution, respectively. (For interpretation of the references to color in this figure legend, the reader is referred to the web version of this article.)

4.2. Time-resolved monitoring with SAXS and DLS

In the second experiment, simultaneous SAXS and DLS time-resolved measurements were performed. SAXS results for R_m and σ evolving with time are shown in Fig. 8. As one can see, clear changes of the mean radius R_m and the standard deviation σ can be observed upon changing synthesis parameters. Here, the Schulz-Zimm size distribution was assumed. The NP size vs. time evolution can be divided into 5 sections corresponding to different sets of synthesis parameters which are summarized in Table 2. For the sake of clearity, size values of NPs synthesized between the sections are not shown. These data points correspond to synthesis parameter sets not defined in Table 2 but arising from sequential adjustment of the pumps to the next parameter set. In the Sections 1–3 the flow rate ratio is 1/3, 1/2 and 1/1.5, respectively and the residence time is 8 min. One can observe a decrease of the particles mean radius with increasing flow rate ratio (1/3 → 1/1.5). In Section 4 the residence time was increased to 22 min at a flow rate

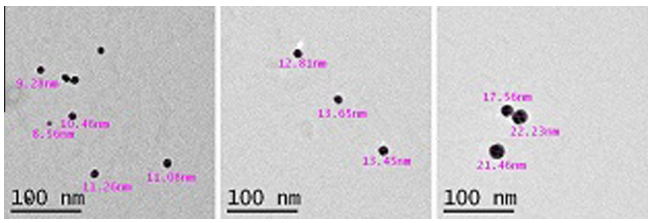

Fig. 7. TEM images of standard gold NPs with diameters of 10 nm, 15 nm and 20 nm.

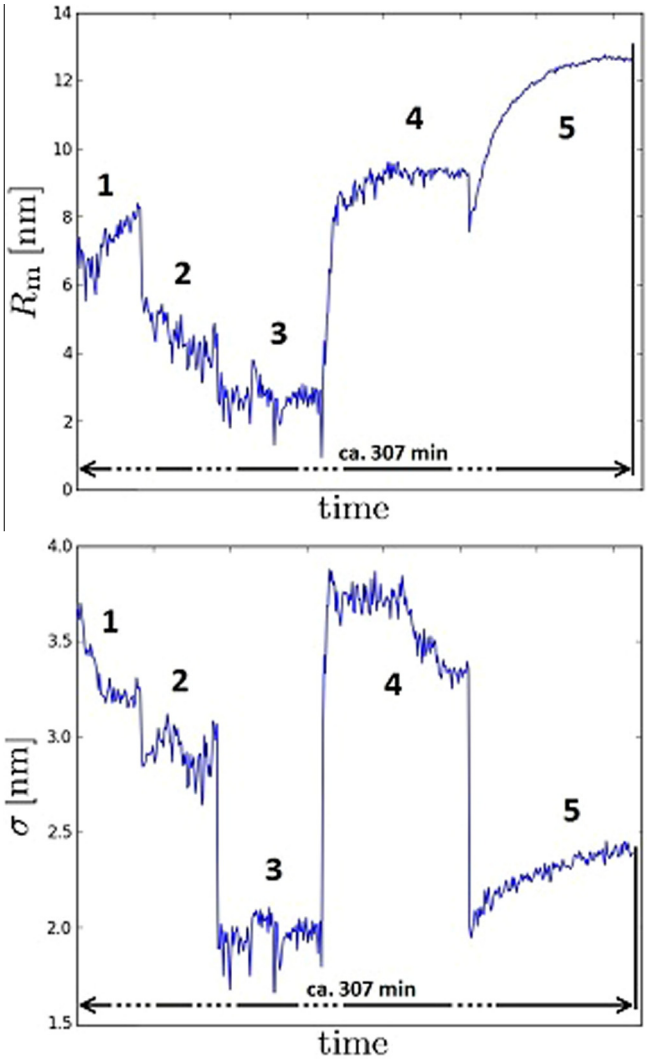

Fig. 8. Evolution of the mean radius R_m and σ during the monitoring experiment.

Table 2
Synthesis parameter sets.

Section	Flow rate ratio F_1/F_2	Residence time [min]
1	30/90	8
2	40/80	8
3	48/72	8
4	15/30	22
5	150/300	2

ratio of 1/2 resulting in bigger particles. In Section 5 the flow rate ratio is 1/2 and the residence time is 2 min. Here, initially no NPs were observable with SAXS indicating that 2 min might be too short to form NPs inside the reactor. Therefore, the flow was stopped to test whether NPs can form inside the capillary. In fact, NP formation and growth was observed inside the capillary. After around 40 min the final mean radius was approximately 12 nm. Moreover, in Section 5 the ratio σ/R_m is the lowest indicating a narrow size distribution. For DLS measurements the flow was stopped at the end of each section. In Table 3 the resulting size values of all measurements are summarized for each section. The SAXS values were determined by evaluating a SAXS curve taken from the middle of a section, respectively, in contrast to DLS values representing

Table 3
Summary of simultaneous SAXS and DLS results for each section with additional *ex situ* DLS and TEM results. All size values are given in units of nm.

Section	SAXS		DLS	DLS (VASCO)	TEM	
	R_m	σ	R_h	R_h	R_m	σ
1	6.6	3.3	22.3	17.7	13.5	4.5
2	3.9	2.9	16.9	16.9	8.6	2.9
3	2.5	1.9	10.7	9.8	–	–
4	9.2	3.5	16.2	17.7	9.8	4.4
5	11.9	2.4	19.9	23.4	14.2	1.8

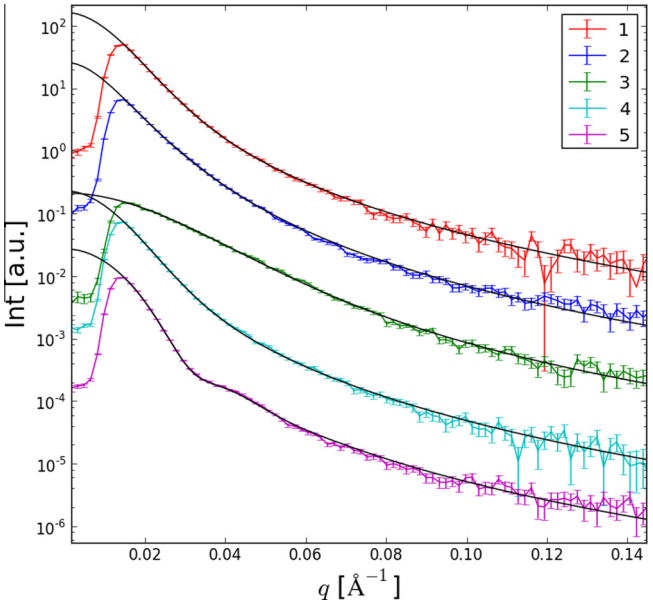

Fig. 9. Representative SAXS curves of SAXS measurements taken from each section. The black lines are the fitted curves.

NPs synthesized at the end of a section. For Section 5 both SAXS and DLS represent almost fully grown NPs. In Fig. 9 representative SAXS curves from each section are shown. As one can see, the shape of the SAXS curves depends on the mean particle size and the width of the size distribution. For example, in the SAXS curve representing Section 5 a second peak emerges at $q = 0.04$ Å^{-1}. This indicates a narrower size distribution compared to the NPs synthesized in the other sections. Additional *ex situ* DLS measurements are also listed. As expected one can see that the DLS values are larger then the SAXS values. This is due to the aforementioned feature of the DLS probe which measures the hydrodynamic size. One can also notice that DSL values show systematic decrease/increase when the SAXS values decrease/increase. Here again the solvation shell is not further investigated. The comparison of the *in situ* DLS with the *ex situ* DLS (VASCO) results shows a maximal deviation of 3 nm in Section 5, confirming that the new DLS device provides reasonable size values. Therefore, we assume that DLS measurements can be performed directly after the synthesis without dilution nor specific sample preparation.

In Fig. 10 images of additional TEM measurements of NPs synthesized in Sections 1, 2, 4 and 5 are shown. The resulting size values after processing the images are also summarized in Table 3. As one can see, TEM provides larger size values indicating that the particles continued to grow after the synthesis. The smallest deviations between SAXS and TEM are in Sections 4 and 5, corresponding to the synthesis parameter sets with the longest and the shortest residence time, respectively.

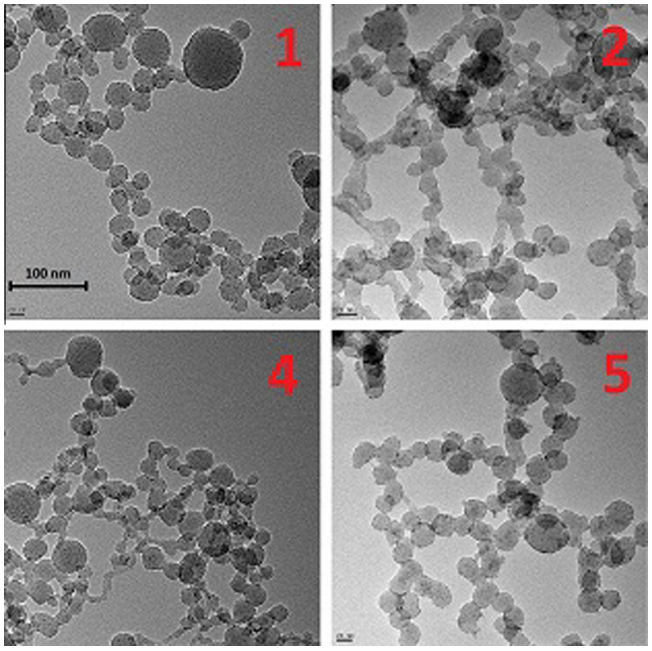

Fig. 10. TEM images of NPs synthesized in Sections 1,2,4 and 5. For Section 3 no proper images could be made due to agglomeration of the NPs.

5. Conclusions

In this work, we have presented a new combined SAXS and DLS experimental setup developed and implemented specifically to perform time-resolved monitoring of NP synthesis. First, we have implemented a new liquid metal anode X-ray source and an optimized X-ray beam collimation system into a Nanostar allowing to improve the X-ray flux by a factor of 10 compared to Brukers rotating anode systems with standard beam collimation. This improvement has lead to a significant reduction of the exposure time without degrading the signal-to-noise ratio. Secondly, an innovative fiber remote DLS probe head has been developed specifically to make *in situ* DLS measurements directly inside the glass capillary located inside the SAXS sample chamber. This unique arrangement was coupled to a microflow reactor and we have demonstrated simultaneous SAXS and DLS measurements to monitor silica NP synthesis with variable synthesis conditions. To the best of our knowledge, this work is the very first experimental demonstration ever reported of the simultaneous use of a laboratory SAXS and DLS for time-resolved NP characterization. Several improvements of the arrangement are already considered; in particular, placing the plane of incidence of the DLS probe head perpendicular to the flow direction. This should reduce drastically the Doppler contribution to the DLS signal and would allow making DLS measurements without stopping the flow. We will also further investigate the correlation between SAXS and DLS results and the parameters of the synthesis reactor. Our goal is to build up a phenomenological model of the synthesis process and define the guidelines for a control loop operation.

Acknowledgments

We would like to thank Amina Wirth Tijani, Boris Pedrono, Cedric Spaas, Didier Frot, Stijn Vandezande, Bastiaan Opperdoes and the electronic and mechanical workshop staff in KU Leuven. We also would like to thank the EU for supporting via the FP7-grant SNOWCONTROL project (263510) and the MOD-ENP-TOX project (310715). J.W.S. thanks the Flemish Hercules stichting for its support in Her/08/25.

References

[1] J. Wang, D. Ye, G. Liang, J. Chang, J. Kong, J. Chen, J. Mater. Chem. B 2 (2014) 4338–4345.
[2] X. Zhou, Y. Yin, L. Wan, Y. Guo, Chem. Commun. 48 (2012) 2198–2200.
[3] J. Zhou, J. Ralston, R. Sedev, D.A. Beattie, J. Colloid Interface Sci. 331 (2009) 251–262.
[4] B.R. Cuenya, Thin Solid Films 518 (2010) 3127–3150.
[5] M. Ahameda, M.S. AlSalhia, M.K.J. Siddiqui, Clin. Chim. Acta 411 (2010) 1841–1848.
[6] B. Chu, T. Liu, J. Nanopart. Res. 2 (2000) 29–41.
[7] H. Boukari, J.S. Lin, M.T. Harris, J. Colloid Interface Sci. 194 (1997) 311–318.
[8] J. Eyssautier, D. Frot, L. Barre, Lagmuir 22 (2012) 11997–12004.
[9] D.J. Tobler, L.G. Benning, Geochim. Cosmochim. Acta 114 (2013) 156–168.
[10] B. Chu, T. Liu, J. Nanopart. Res. 2 (2000) 29–41.
[11] O. Hemberg, M. Otendal, H.M. Hertz, Appl. Phys. Lett. 83 (2003) 1483–1485.
[12] D.H. Larsson, U. Lundström, U.K. Westermark, M.A. Henriksson, A. Burvall, H.M. Hertz, Med. Phys. 40 (2013) 021909.
[13] <https://www.excillum.com>.
[14] A. Kleine, SCATEX The new scatterfree pinholes, <www.incoatec.de>.
[15] J.S. Pedersen, Appl. Crystallogr. 37 (2004) 369–380.
[16] W. Stober, A. Fink, E. Bohn, J. Colloid Interface Sci. 26 (1968) 62–69.
[17] D.L. Green, S. Jayasundara, Y. Lam, M.T. Harris, J. Non-Cryst. Solids 315 (2003) 166–179.
[18] J.S. Pedersen, in: P. Lindner, Th. Zemb (Eds.), Neutrons, X-Rays and Light, Elsevier Science B.V., 2002. p. 391.
[19] M. Kotlarchyk, S. Chen, J. Chem. Phys. 79 (1983) 2461.
[20] B.J. Berne, R. Pecora, Dynamic Light Scattering with Applications to Chemistry, Biology and Physics, Dover Publications Inc., 2000.